Electronic Supplementary Information

Epitaxial synthesis of ultrathin β-In_2Se_3/MoS_2 heterostructures with high visible/near-infrared photoresponse

Zixing Zou‡[a], Dong Li‡[a], Junwu Liang[b], Xuehong Zhang[a], Huawei Liu[a], Chenguang Zhu[a], Xin Yang[a], Lihui Li[a], Biyuan Zheng[a], Xingxia Sun[a], Zhouxiaosong Zeng[a], Jiali Yi[a], Xiujuan Zhuang[a], Xiao Wang[a], and Anlian Pan*[a]

[a]Key Laboratory for Micro-Nano Physics and Technology of Hunan Province, College of Materials Science and Engineering, School of Physics and Electronics, and State Key Laboratory of Chemo/Biosensing and Chemometrics, Hunan University, Changsha, Hunan 410082, P. R. China

[b]School Physics and Telecommunication Engineering, Yulin Normal university, Yulin, Guangxi 537000, P. R. China

*Corresponding authors: anlian.pan@hnu.edu.cn

‡These authors contributed equally to this study.

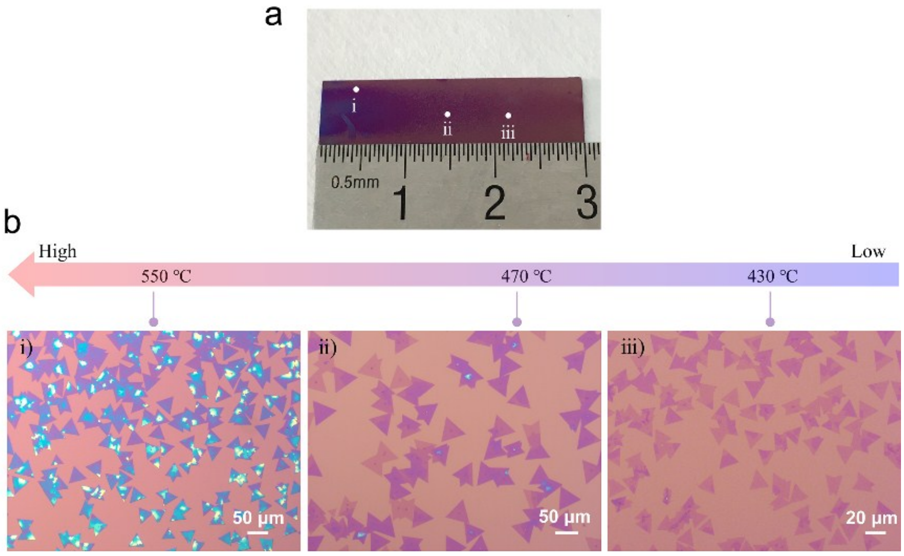

Fig.S1 Temperature dependent growth behavior of In_2Se_3/MoS_2 heterostructures. (a) Low magnification image of the achieved In_2Se_3/MoS_2 heterostructures on SiO_2/Si substrate. (b) The magnified morphology images of In_2Se_3/MoS_2 heterostructures acquired from i, ii, iii positions in (a), where the temperatures measured at three positions are 550 °C, 470 °C and 430 °C, respectively.

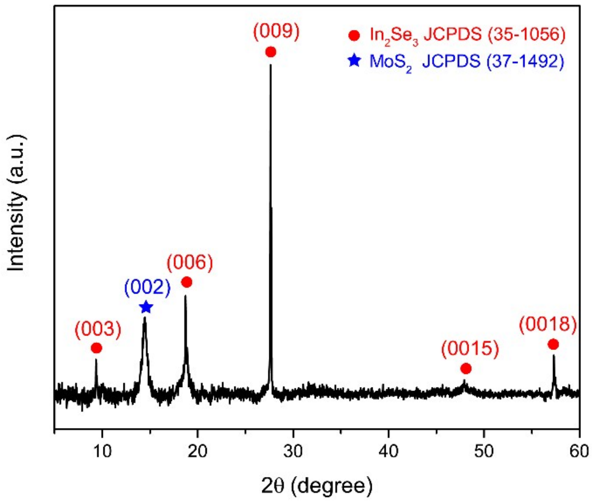

Fig.S2 X-ray diffraction (XRD) spectrum of In_2Se_3/MoS_2 heterostructures. The peak positions can be indexed to β-In_2Se_3 (JCPDS 35-1056) and MoS_2 (JCPDS 37-1492), respectively. Such result confirms the high crystal quality and phase purity of the achieved samples.

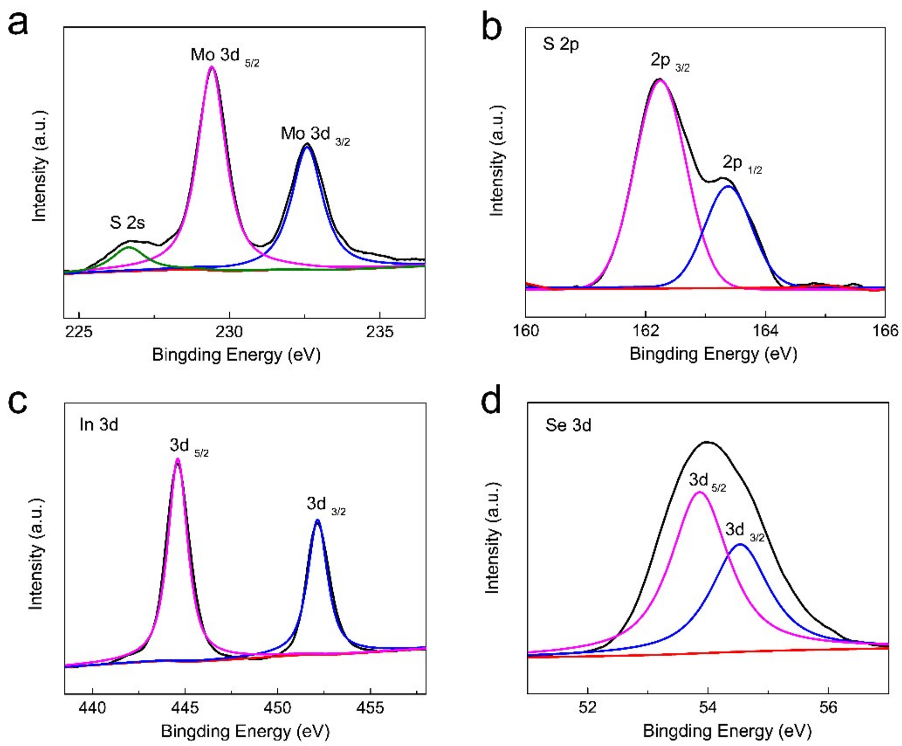

Fig. S3 X-ray photoelectron spectroscopy (XPS) of In_2Se_3/MoS_2 heterostructures. (a) The binding energies for Mo $3d_{5/2}$ and Mo $3d_{3/2}$ are located at 229.4 eV and 232.5 eV, respectively. (b) The binding energies for S $2p_{3/2}$ and S $2p_{1/2}$ are located at 162.2 eV and 163.4 eV, corresponding well with the value of MoS_2. (c) The spectrums of In $3d_{5/2}$ and In $3d_{3/2}$ are located at 445.6eV and 452.1 eV respectively. (d) The peaks at 53.8eV and 54.6 eV belong to Se $3d_{5/2}$ and Se $3d_{3/2}$, which can be assigned to the previous reported value of In_2Se_3. According to the above results, we confirm that the heterostructures have formed by pure constituents without alloying.

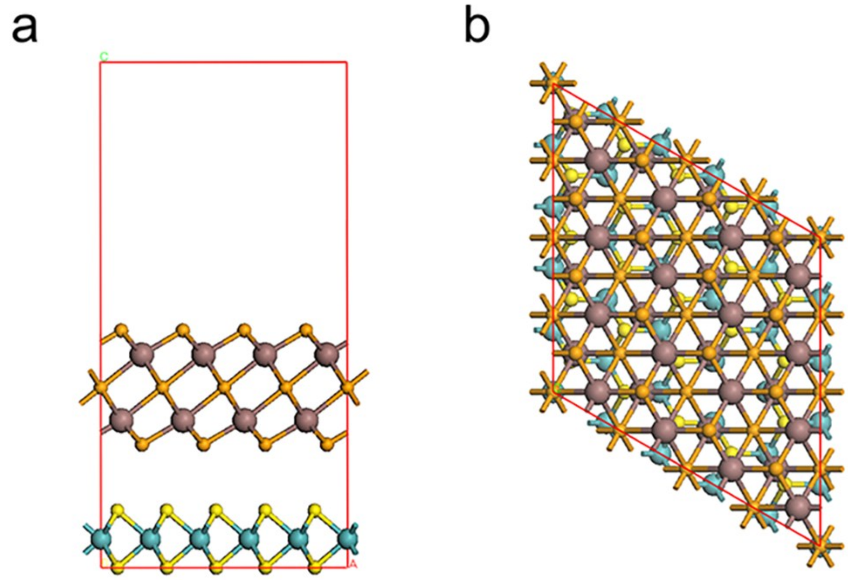

Fig.S4 Atomic structure of In_2Se_3/MoS_2 heterostructure supercell with side (a) and top (b) views. Single layer In_2Se_3 possesses a quintuple layer (QLs) structure, where the Se–In–Se–In–Se atomic sheets are held together by strong in-plane covalent bond.

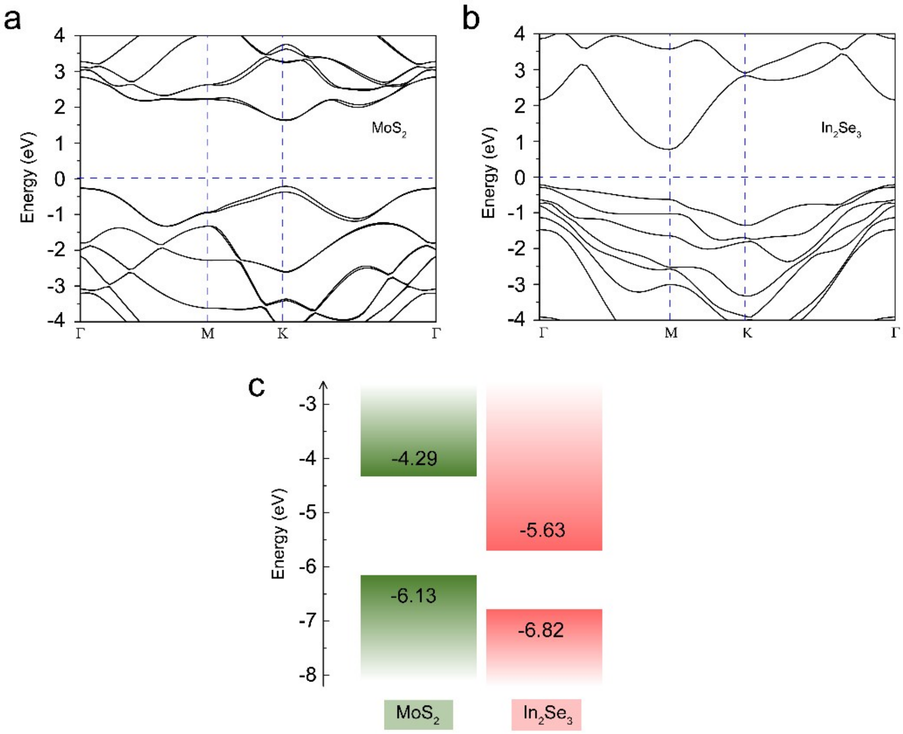

Fig.S5 Electronic band structure of (a) In_2Se_3 and (b) MoS_2. As can be seen, monolayer MoS_2 has direct bandgap while monolayer In_2Se_3 possesses indirect bandgap. (c) Band alignment of the In_2Se_3/MoS_2 heterostructure.

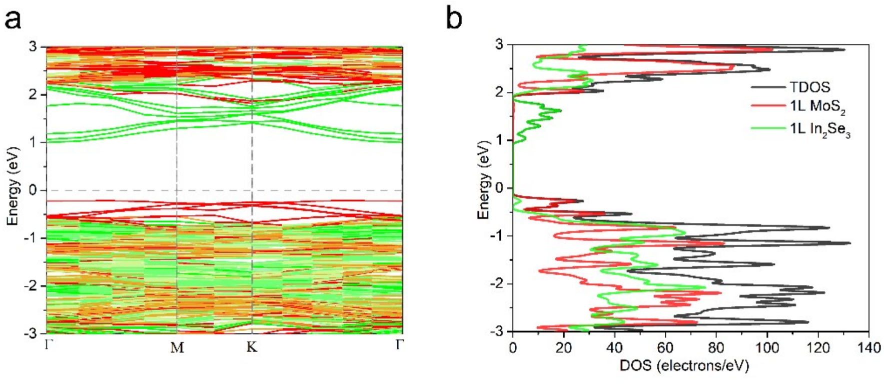

Fig. S6 (a) Band structure and (b) density of states of the In_2Se_3/MoS_2 heterostructure. The band structure and bandgap value of heterostructure change when compared with monolayer MoS_2 and monolayer In_2Se_3. The conduction band minimum (CBM) is dominated by In_2Se_3 and the valence band maximum (VBM) is mainly composed of MoS_2, revealing the weak interlayer coupling.

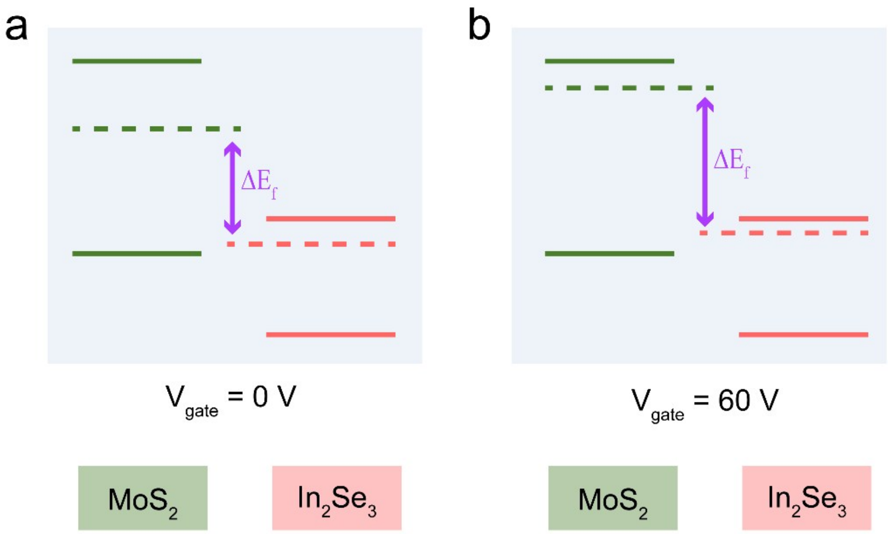

Fig. S7 Band alignments of MoS_2 and In_2Se_3 at gate voltage of (a) 0 V and (b) 60 V.

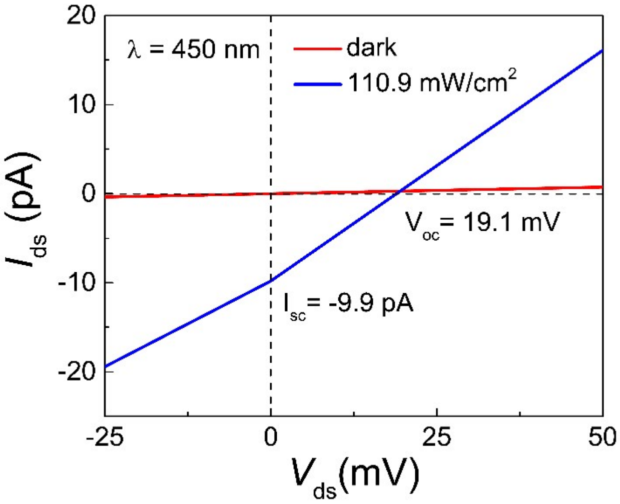

Fig. S8 Photovoltaic effect of In_2Se_3/MoS_2 heterostructures under 450 nm illumination at power density of 110.9 mW/cm^2

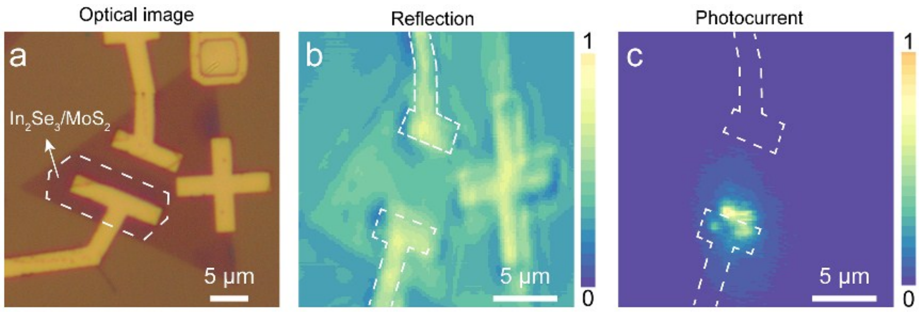

Fig. S9 (a) Optical microscope image of the device. (b) Reflection image of the device (c) Photocurrent mapping of the device.

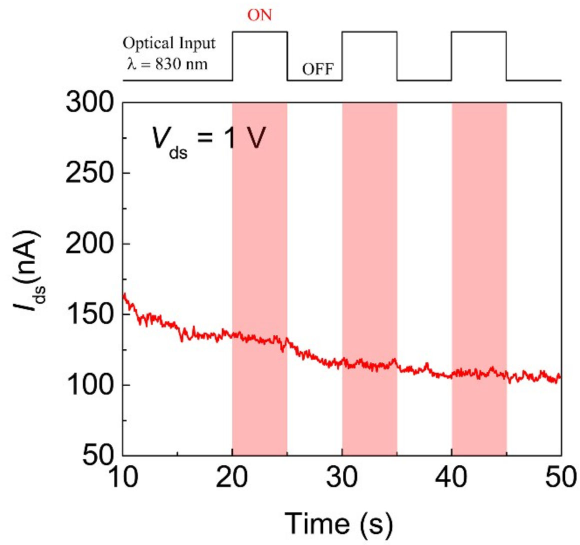

Fig.S10 Time-resolved photoresponse of the device based on monolayer MoS_2 under 830 nm laser illumination with power density of 214.3 mW/cm^2.

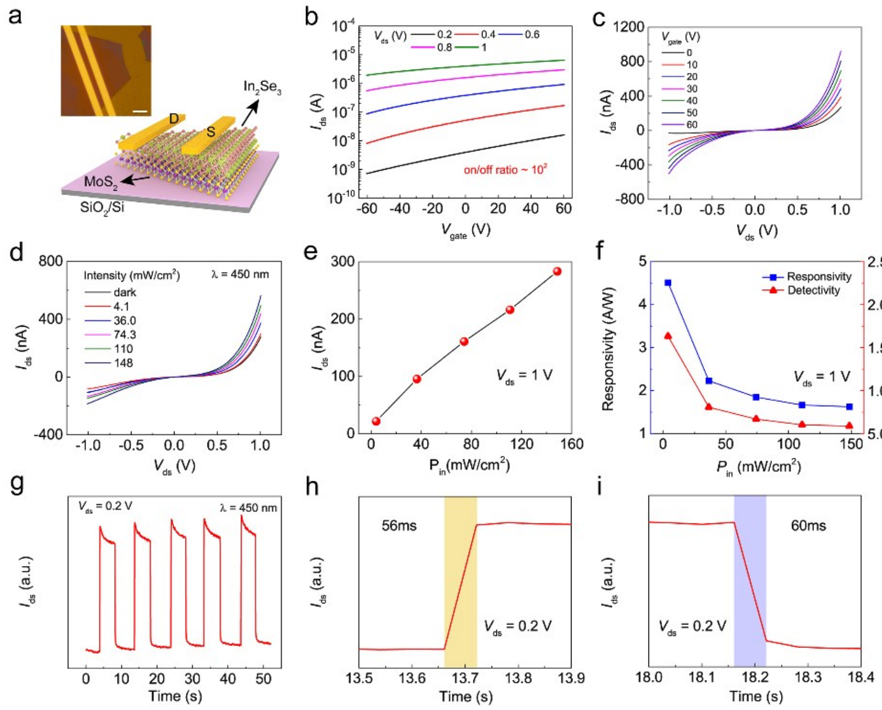

Fig.S11 Electrical and photoelectronic properties of few layer In_2Se_3/MoS_2 heterostructures. (a) Schematic illustration of the In_2Se_3/MoS_2 vdWs heterostructure device on a SiO_2/Si substrate. Inset is an optical image of as-fabricated In_2Se_3/MoS_2 heterostructure device. Scale bar, 5 μm. (b) transfer curves with increasing bias voltages from 0.2 V to 1 V. (c) I_{ds}-V_{ds} curves at various back-gated voltages from 0 V to 60 V. (d) I_{ds}-V_{ds} curves in dark and under 450 nm illumination at different incident power densities. (e) Power dependent photocurrent curve at bias voltage of 1 V. (f) Power dependent responsivity and detectivity curves at bias voltage of 1 V. (g) Time-resolved photoresponse of the device under the laser turned on/off. (450 nm, 110 mW/cm^2, V_{ds} = 0.2 V). (h,i) The rise and decay times of the photocurrent at bias voltage of 1 V.

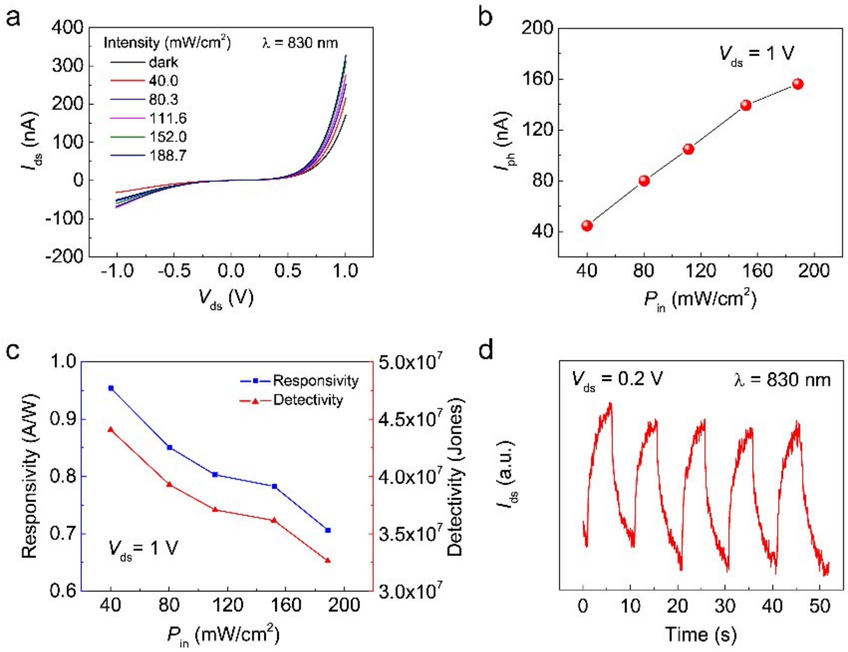

Fig.S12 Photoresponse characterizations of few layer In_2Se_3/MoS_2 heterostructures under 830 nm laser illumination. (a) I_{ds}-V_{ds} curves of the photodetector measured in dark and under different power densities. (b) Photocurrent as a function of illumination power density at the bias voltage of 1 V. (c) Responsivity and detectivity as a function of illumination power density at the bias voltage of 1 V. (d) Time-resolved photoresponse of the device (830 nm, 188.7 mW/cm^2, V_{ds} = 1 V). (e,f) The rise and decay times of the photocurrent measured at V_{ds} = 0.2 V.